The Paf1 complex is required for RNA polymerase II removal in response to DNA damage

Feilong Chen[a,1,2] (iD), Beibei Liu[a,1], Hao Zhou[a], and Jiafu Long[a,b,2] (iD)

Rpb1, the largest subunit of RNA polymerase II (RNAPII), is rapidly polyubiquitinated and degraded in response to DNA damage; this process is considered to be a "mechanism of last resort" employed by cells. The underlying mechanism of this process remains elusive. Here, we uncovered a previously uncharacterized multistep pathway in which the polymerase-associated factor 1 (Paf1) complex (PAF1C, composed of the subunits Ctr9, Paf1, Leo1, Cdc73, and Rtf1) is involved in regulating the RNAPII pool by stimulating Elongin-Cullin E3 ligase complex-mediated Rpb1 polyubiquitination and subsequent degradation by the proteasome following DNA damage. Mechanistically, Spt5 is dephosphorylated following DNA damage, thereby weakening the interaction between the Rtf1 subunit and Spt5, which might be a key step in initiating Rpb1 degradation. Next, Rad26 is loaded onto stalled RNAPII to replace the Spt4/Spt5 complex in an RNAPII-dependent manner and, in turn, recruits more PAF1C to DNA lesions via the binding of Rad26 to the Leo1 subunit. Importantly, the PAF1C, assembled in a Ctr9-mediated manner, coordinates with Rad26 to localize the Elongin-Cullin complex on stalled RNAPII, thereby inducing RNAPII removal, in which the heterodimer Paf1/Leo1 and the subunit Cdc73 play important roles. Together, our results clearly revealed a new role of the intact PAF1C in regulating the RNAPII pool in response to DNA damage.

Paf1 complex | RNA polymerase II removal | Rad26 | Spt4/Spt5 complex | DNA damage

RNA polymerase II (RNAPII) transcribes a gene from the transcription start site to generate a nascent RNA through a process including the steps of initiation, elongation, and termination. Recently, the early elongation stage at promoter-proximal sites was identified as an important rate-limiting step of transcription. Substantial research effort in metazoan cells contributed to the understanding of transcriptional regulation at promoter-proximal sites (1–4). RNAPII molecules often pause at promoter-proximal sites after initiating transcription from a promoter, and this pause is maintained by the protein complex composed of NELF (negative elongation factor) and 5,6-dichloro-1-β-D-ribofuranosylbenzimidazole sensitivity-inducing factor (DSIF) (the human ortholog of the yeast Spt4/Spt5 complex) (5–7). The release of paused RNAPII is regulated by the polymerase-associated factor 1 (Paf1) complex (PAF1C) and the positive transcription elongation factor b (P-TEFb) (3, 8, 9). P-TEFb phosphorylates Spt5 and NELF, which triggers DSIF to function as a positive elongation factor and NELF to dissociate from RNAPII (10–12). Subsequently, the elongation factors PAF1C and Spt6 associate with the RNAPII machinery for fast elongation throughout the gene in concert with DSIF (13–17).

Like early elongation at promoter-proximal sites, productive elongation in gene bodies is not smooth and continuous, partially because of RNAPII stalling at bulky DNA lesions (18–21). In response to DNA damage, transcription elongation is severely inhibited (22–24), and RNAPII molecules are persistently stalled at DNA lesions, which might induce apoptosis or cell death (24, 25). To survive DNA damage, cells employ multiple pathways to ensure transcription recovery (26, 27). The transcription-coupled DNA repair (TCR) pathway efficiently removes transcription-blocking DNA lesions from the template strand of active genes (reviewed in ref. 28–30), a process initiated by recognition of DNA lesions by the protein Cockayne syndrome B protein (CSB) (the human ortholog of yeast Rad26) in an elongating RNAPII-dependent manner (31–33). Recently, several studies have reported the interesting observation that in both yeast and humans, DSIF is exchanged for CSB as the state of RNAPII changes from rapid elongation to pausing at DNA lesions (20, 34–36). However, the detailed mechanism of this phenomenon remains elusive. As an alternative pathway to TCR, Rpb1, the largest subunit of RNAPII, is ubiquitinated and degraded following DNA damage, leading to disassembly and removal of damage-stalled RNAPII, which is

Significance

The highly conserved polymerase-associated factor 1 complex (PAF1C) is composed of five core subunits (Ctr9, Paf1, Cdc73, Rtf1, and Leo1) and involved in all stages of RNA polymerase II (RNAPII)-mediated transcription. This study involves biochemical and mechanistic insights into the role of PAF1C subunits in regulating the RNAPII pool in response to DNA damage via a previously uncharacterized multistep pathway. The data from both *in vivo* and *in vitro* assays clearly revealed that PAF1C orchestrates the exchange of Spt5 and Rad26 via the Rtf1 subunit and the recruitment of the Elongin-Cullin E3 complex to stalled RNAPII via the heterodimer Paf1/Leo1 in concert with Rad26, thereby facilitating RNAPII removal.

considered the "mechanism of last resort" (reviewed in ref. 37). This pathway should be precisely regulated to prevent unnecessary Rpb1 degradation, which might affect cell survival (24). In budding yeast, the Elongin-Cullin E3 ligase complex, containing the subunits cullin 3 (Cul3), RING finger protein Roc1 (Rbx1), elongin C (Elc1), and elongin A (Ela1), is responsible for adding lysine 48-linked ubiquitin chains to Rpb1 following DNA damage (38–40). Moreover, prior studies have shown that the interaction between the Elongin-Cullin complex and RNAPII is weak and might be stabilized by Def1, a Rad26-binding protein (27, 41). Despite these great advances, the mechanism by which the Elongin-Cullin E3 ligase specifically recognizes the substrate RNAPII is not very clear.

The highly conserved PAF1C is composed of five core subunits (Ctr9, Paf1, Cdc73, Rtf1, and Leo1), with an additional subunit (Ski8) in human PAF1C, and is involved in all stages of RNAPII-mediated transcription and RNA processing (reviewed in ref. 42–44), especially in transcriptional regulation at promoter-proximal sites, as described above. Intriguingly, PAF1C has been recently reported to interact with RNAPII in a CSB-dependent manner under DNA damage conditions and participate in restoring transcription after DNA damage repair (20). Unlike the DSIF complex, PAF1C is involved not only in the assembly of the activated transcriptional RNAPII machinery (during fast elongation) (13, 15–17) but also in binding the TCR-initiation factor CSB (during RNAPII stalling at DNA lesions) (20, 36). These findings prompted us to ask whether PAF1C plays a role in the transition of the transcriptional state from fast elongation to stalling. Additionally, a previous work showed that chromatin-bound RNAPII is degraded in a PAF1C-dependent manner in cells exposed to hydroxyurea (a chemical causing replication stress) (45), and yet the mechanisms remain unclear. Here, we provide detailed biochemical and mechanistic insights into the role of PAF1C in orchestrating the exchange of Spt5 and Rad26 as well as RNAPII removal at DNA lesions following DNA damage.

Results

Each Subunit of PAF1C Is Involved in Regulating the RNAPII Pool after DNA Damage.
During DNA damage, stalled or arrested RNAPII is ubiquitinated and thus degraded by the proteasome, which is considered to be a mechanism of last

resort for survival (reviewed in ref. 37). The largest subunit of RNAPII, Rpb1, can quickly undergo polyubiquitination and degradation in response to the ultraviolet-mimetic compound 4-nitroquinoline-1-oxide (4-NQO) (38, 39, 46). A prior study showed that in yeast lacking the *PAF1* gene, Rpb1 is not degraded upon hydroxyurea-induced replication stress (45). These observations led us to investigate the role of Paf1 in Rpb1 degradation upon 4-NQO-induced transcriptional stress. Notably, following 4-NQO treatment, Rpb1 was quickly degraded in the wild-type (WT) yeast strain but not in the strain with *PAF1* gene deletion (*paf1Δ*) (lanes 6 to 10 compared with lanes 1 to 5 in Fig. 1*A*; Fig. 1*B*). Based on accumulating results demonstrating that the functionally conserved PAF1C acts as a diverse hub to regulate all stages of RNAPII-mediated transcription and RNA processing (reviewed in Refs (42–44).) combined with our observation that intact PAF1C is required to efficiently stimulate Rad6/Bre1-mediated monoubiquitination of histone H2B (H2Bub) (47), we speculated that subunits of PAF1C in addition to Paf1 might also play a role in DNA damage–induced Rpb1 degradation. Accordingly, yeast strains with deletion of either the *LEO1*, *CTR9*, *CDC73*, or *RTF1* gene were used to evaluate the protein level of Rpb1 after DNA damage (Fig. 1*A* and *SI Appendix*, Table S1).

Intriguingly, we found that deletion of either the *LEO1*, *CTR9*, or *CDC73* gene in strains suppressed Rpb1 degradation (lanes 11 to 15, 16 to 20, or 21 to 25, respectively, compared to lanes 1 to 5 in Fig. 1*A*; Fig. 1*B*). These results indicated that the subunits Ctr9, Paf1, Leo1, and Cdc73, which are stably associated within PAF1C in most species (42, 43, 48–50), promote Rpb1 degradation in response to DNA damage. This observation, together with the findings showing that Ctr9 is a key scaffold protein for yeast PAF1C assembly and functional regulation (49. 51), suggested that deletion of the Ctr9 subunit may result in disruption of intact PAF1C assembly and thus lead to defects in Rpb1 degradation in the *ctr9Δ* strain. The mechanisms by which the loss of the *PAF1*, *LEO1*, or *CDC73* gene in yeast causes defects in DNA damage–induced Rpb1 degradation need to be further explored (for a detailed study, see Figs. 2–4 and *SI Appendix*, Fig. S5 and the related text). Intriguingly, we noted that the loss of the *RTF1* gene (*rtf1Δ*) in yeast accelerated the degradation of Rpb1 (lanes 26 to 30 compared to lanes 1 to 5 in Fig. 1*A*; Fig. 1*B*), which is different from the effects of loss of the other four subunits of PAF1C
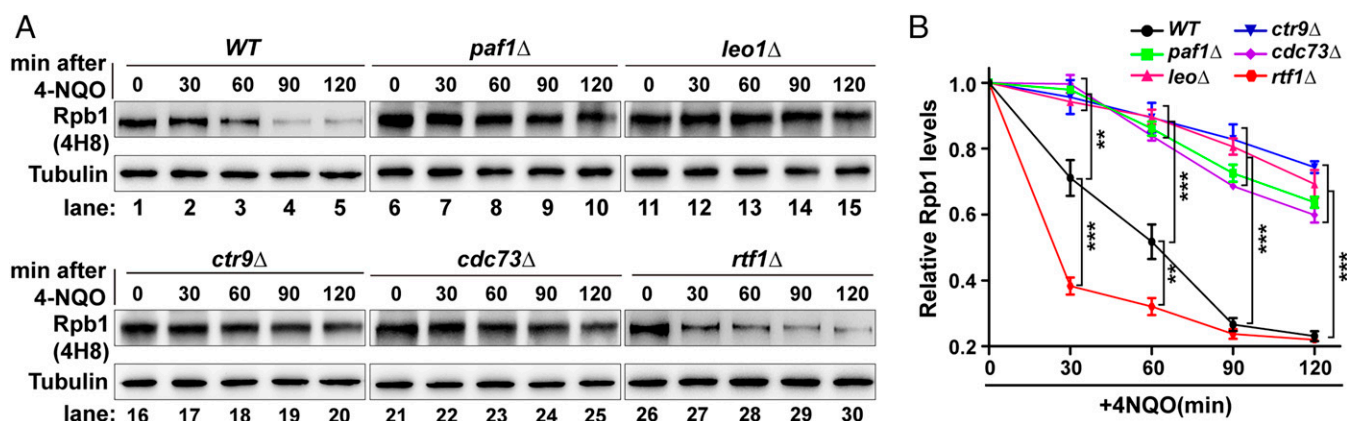
Fig. 1. Each subunit of PAF1C is involved in regulating the RNAPII pool after DNA damage. (*A*) In vivo DNA damage–induced Rpb1 degradation assay. Logarithmically growing yeast cells were treated with 4-NQO at a final concentration of 5 μg/mL for the indicated times. Samples were prepared by alkaline extraction and analyzed by sodium dodecyl sulfate-polyacrylamide gel electrophoresis (SDS–PAGE) and Western blotting. The 4H8 antibody was used to visualize global Rpb1 protein levels. (*B*) Quantification of the protein levels of Rpb1 shown in *A*. The intensity of the Rpb1 bands was quantified using ImageJ software, and the intensity at time 0 was used for normalization. The error bars indicate the means and SDs (means ± SDs) (*n* = 3 separate experiments). **P < 0.01, ***P < 0.001.

Fig. 2. The binding of Ela1 to the heterodimer Paf1/Leo1 is important for DNA damage–induced Rpb1 polyubiquitination and degradation. (*A*) The purified intact Elongin-Cullin E3 ligase complex mediates the ubiquitination of the substrate RNAPII. An in vitro ubiquitination assay was performed as indicated. The reactants were incubated for 120 min at 30 °C and analyzed by 6% SDS–PAGE. The membrane was im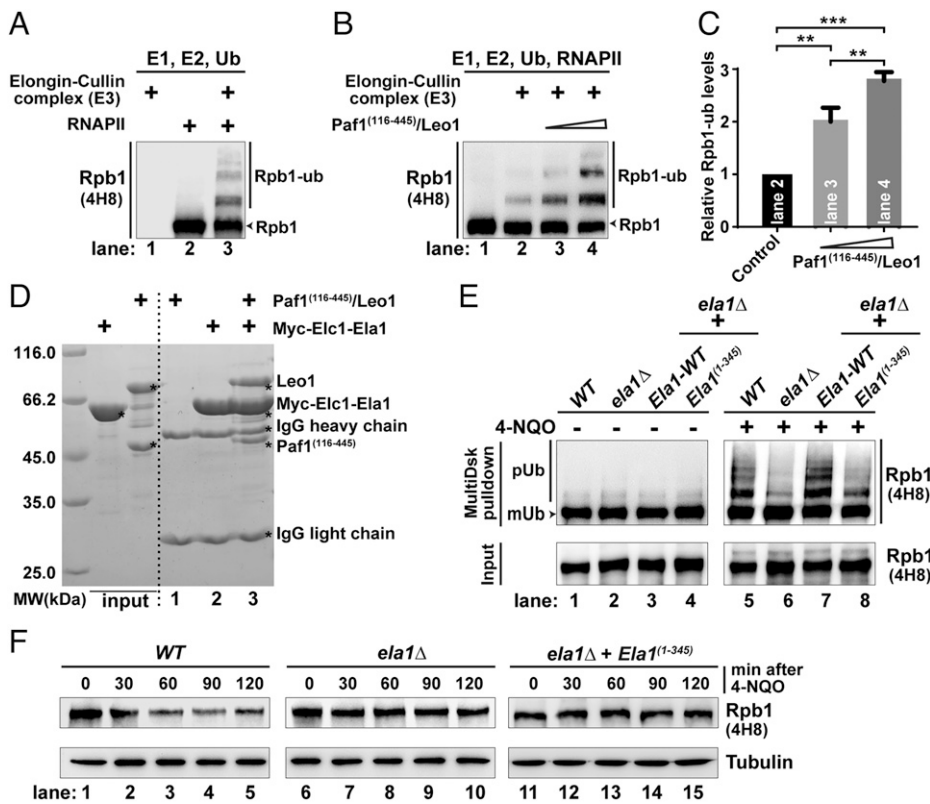munoblotted with the 4H8 antibody to specifically detect both Rpb1 and Rpb1-ub (polyubiquitinated Rpb1). (*B* and *C*) The heterodimer Paf1/Leo1 promotes Elongin-Cullin complex–mediated Rpb1 ubiquitination in a dose-dependent manner. (*B*) An in vitro ubiquitination assay was performed in the presence of incremental amounts of the Paf1$^{(116-445)}$/Leo1 complex (lanes 3 and 4, final concentrations of 1 and 2 μM, respectively). The reactants were incubated for 120 min at 30 °C and analyzed by 6% SDS–PAGE. The membrane was immunoblotted with the 4H8 antibody to specifically detect both Rpb1 and Rpb1-ub. (*C*) Quantitative analysis of the in vitro ubiquitination assay results in *B*. The band intensity of Rpb1-ub was quantified using ImageJ software. A control (lane 2 in *B*) was used for normalization. The error bars indicate the means and SDs (means ± SDs) (n = 3 separate experiments). **P < 0.01, ***P < 0.001. (*D*) Ela1 directly interacts with the heterodimer Paf1/Leo1. Pull-down assays of purified Myc-Elc1-Ela1 with the Paf1$^{(116-445)}$/Leo1 complex were performed. Anti-Myc-tag agarose beads bound to Myc-Elc1-Ela1 were incubated with the Paf1$^{(116-445)}$/Leo1 complex as indicated for 1 h at 4 °C. The prepared samples were separated by SDS–PAGE, and the gel was subjected to Coomassie blue staining. (*E*) The extreme C terminus of Ela1 is important for DNA damage–induced Rpb1 ubiquitination in vivo. GST beads bound to GST-Multi-Dsk2 were incubated with various yeast cell lysates as indicated for 2 h at 4 °C. The prepared samples were separated by SDS–PAGE and then subjected to immunoblotting with the 4H8 antibody to specifically detect Rpb1 ubiquitination. pUb, polyubiquitination; mUb, monoubiquitination. (*F*) Rpb1 degradation was suppressed in a yeast strain lacking the extreme C terminus of Ela1 following DNA damage. Logarithmically growing yeast cells were treated with 4-NQO at a final concentration of 5 μg/mL for the indicated times. Samples were prepared by alkaline extraction and analyzed by SDS–PAGE and Western blotting. The 4H8 antibody was used to visualize global Rpb1 protein levels.

(lanes 26 to 30 compared to lanes 6 to 10, 11 to 15, 16 to 20, and 21 to 25 in Fig. 1*A*; Fig. 1*B*), indicating that the Rtf1 subunit may have an important role in DNA damage–induced Rpb1 degradation (for a detailed study, see Fig. 5 and the related text). Together, these results demonstrated that each subunit of yeast PAF1C may play a role in regulating the RNAPII pool after DNA damage.

The Binding of Ela1 to the Heterodimer Paf1/Leo1 Is Important for DNA Damage–Induced Rpb1 Polyubiquitination and Degradation. Prior studies demonstrated that the yeast Elongin-Cullin E3 ligase complex, containing the subunits Ela1, Elc1, Rbx1, and Cul3, is responsible for adding lysine 48–linked ubiquitin chains to Rpb1 for its proteasomal degradation in response to DNA damage (38–40). Ela1, the substrate receptor for the Elongin-Cullin E3 ligase complex, contains a conserved "BC-box" in its N-terminal region (*SI Appendix*, Fig. S1*A*). Intriguingly, we found that the Ela1(3M) mutant, in which three highly conserved residues (Leu4, Cys8, and Leu12) in the BC-box were replaced with aspartic acid, did not bind to Elc1 and Cul3 (*SI Appendix*, Fig. S1 *B* and *C*) and that re-expression of the Ela1(3M) mutant in the *ela1Δ* strain diminished Rpb1 ubiquitination (*SI Appendix*, Fig. S1*D*) and disrupted Rpb1 degradation (*SI Appendix*, Fig. S1*E*). Moreover, notably, the protein level of Ela1(3M) was comparable to that of Ela1-WT (lane 4 compared to lane 1 in *SI Appendix*, Fig. S2*A*). These findings, combined with our data showing that the subunits Paf1 and Leo1 of yeast PAF1C are involved in DNA damage–induced Rpb1 degradation (Fig. 1) and the observations that Paf1 and Leo1 function as a heterodimer for

substrate recognition during Rad6/Bre1-mediated H2Bub (47) and that the interactions between human Paf1 or Leo1 and the Elongin-Cullin complex can be detected in vivo (52), led us to speculate that the heterodimer Paf1/Leo1 in yeast PAF1C may bind to the Elongin-Cullin E3 ligase complex and is involved in Elongin-Cullin complex–mediated Rpb1 ubiquitination and degradation. To test this hypothesis, it was necessary to generate an intact Elongin-Cullin complex and establish a defined in vitro ubiquitination system. Accordingly, we found by a coimmunoprecipitation (co-IP) assay that an N-terminal fragment of Ela1 (amino acids [aa] 1 to 143, Ela1$^{(1-143)}$) was sufficient for Ela1 binding to Elc1 (*SI Appendix*, Fig. S3 *A* and *B*). Moreover, for the purpose of stabilizing the recombinant protein Ela1$^{(1-143)}$, Elc1 was fused to the N terminus of Ela1$^{(1-143)}$ with a tobacco etch virus–cleavable segment (here named Elc1-Ela1$^{(1-143)}$; "-" denotes proteins in a single-chain fusion here and in similar nomenclature introduced hereafter). Notably, the results from analytical size-exclusion column and analytical ultracentrifugation showed that the Elc1/Ela1$^{(1-143)}$ complex (where "/" denotes protein complexes with separate chains here and similar structures introduced hereafter) and the single-chain fusion Elc1-Ela1$^{(1-143)}$ have similar behaviors (*SI Appendix*, Fig. S3 *C* and *D*). Subsequently, Elc1-Ela1$^{(1-143)}$, Cul3, and Rbx1 were coexpressed, purified, and assembled into a Cul3/Rbx1/Elc1-Ela1$^{(1-143)}$ complex, as indicated by their coelution from an analytical size-exclusion column (*SI Appendix*, Fig. S3*E*). Finally, using a similar coexpression strategy, we purified an intact thioredoxin (Trx)-tagged Elongin-Cullin complex (Trx-Cul3/Trx-Rbx1/Trx-Elc1-Ela1 complex, lane 3 in *SI Appendix*, Fig. S3*F*). To test the E3 ligase activity
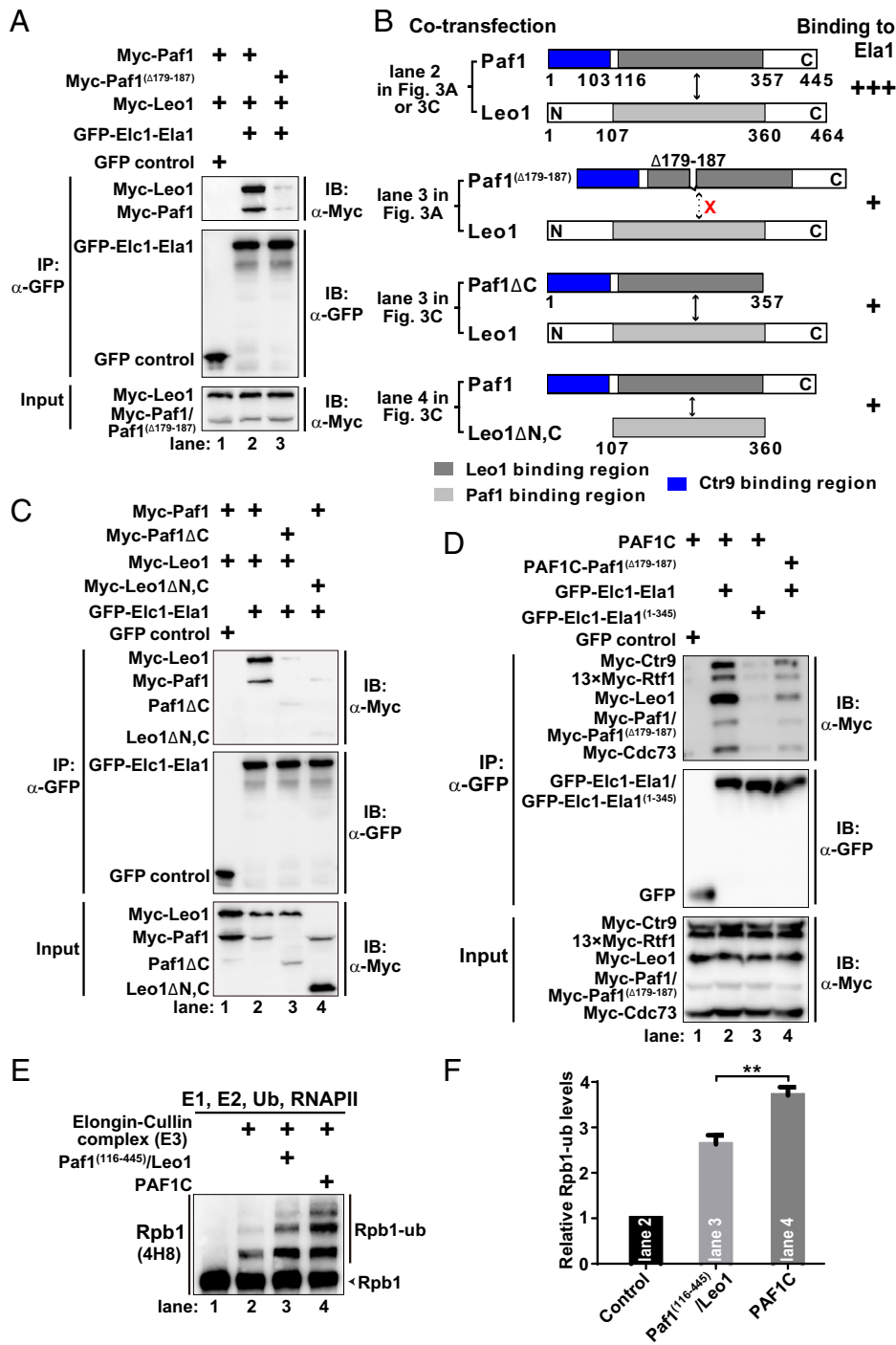
Fig. 3. Each subunit of the heterodimer Paf1/Leo1 is important for its binding to Ela1. (*A*) Heterodimer formation is important for the binding of the Paf1/Leo1 complex to Ela1. Co-IP experiments were performed to evaluate the binding of Elc1-Ela1 to the WT and mutant Paf1/Leo1 heterodimer. Extracts were prepared from HEK293T cells transfected with various combinations of plasmids, as indicated. The *Bottom* panel shows 5% of the Myc-tagged fusion proteins for each IP. (*B*) Summary of the results in *A* and *C*. A schematic representation of various combinations of the Paf1/Leo1 complex components is shown. Greater numbers of "+"s correlate with higher Ela1 binding affinity for the corresponding Paf1/Leo1 complex. (*C*) The C terminus of Paf1 and the N- and C terminus of Leo1 are involved in its binding to Elc1-Ela1. Co-IP experiments were performed to evaluate the binding of Elc1-Ela1 to the Paf1/Leo1 complex or various Paf1/Leo1 complex truncations. Extracts were prepared from HEK293T cells transfected with various combinations of plasmids, as indicated. The *Bottom* panel shows 5% of the Myc fusion proteins for each IP. (*D*) PAF1C binding to Ela1 via the heterodimer Paf1/Leo1. Co-IP experiments were performed to evaluate the binding of full-length Ela1 and truncated Ela1$^{(1-345)}$ (both fused to Elc1; referred to as Elc1-Ela1 and Elc1-Ela1$^{(1-345)}$, respectively) to PAF1C or PAF1C containing the Paf1$^{(Δ179-187)}$ mutant (PAF1C-Paf1$^{(Δ179-187)}$). Extracts were prepared from HEK293T cells transfected with various combinations of plasmids, as indicated. The *Bottom* panel shows 5% of the Myc fusion proteins for each IP. (*E* and *F*) Intact PAF1C stimulates Elongin-Cullin complex–mediated Rpb1 ubiquitination much more efficiently than the heterodimer Paf1/Leo1. (*E*) An in vitro ubiquitination assay was performed by adding the heterodimer Paf1/Leo1 (lane 3) or PAF1C (lane 4), as indicated, at a final concentration of 2 μM. The reactants were incubated for 120 min at 30 °C and analyzed by 6% SDS–PAGE. The membrane was immunoblotted with the 4H8 antibody to specifically detect both Rpb1 and Rpb1-ub. (*F*) Quantitative analysis of the in vitro ubiquitination assay results in *E*. The band intensity of Rpb1-ub was quantified using ImageJ software. A control (lane 2 in *E*) was used for normalization. The error bars indicate the means and SDs (means ± SDs) (*n* = 3 separate experiments). **$P < 0.01$.

of the purified Elongin-Cullin complex in vitro, we prepared the substrate RNAPII (lane 5 in *SI Appendix*, Fig. S3*F*) and various components of the ubiquitination system (E1 (Uba1), E2 (Cdc34), and ubiquitin (Ub); lanes 1, 2 and 4, respectively, in *SI Appendix*, Fig. S3*F*). Notably, RNAPII was efficiently ubiquitinated in the presence of the purified recombinant Elongin-Cullin E3 ligase complex (lane 3 in Fig. 2*A*). Consistent with this finding, a prior study reported that the human Elongin-Cullin E3 complex is capable of mediating Rpb1 ubiquitination directly (53). The single-chain fusion Elc1-Ela1 was used in the following experiments unless stated otherwise.

To test the role of the heterodimer Paf1/Leo1 in Elongin-Cullin complex–mediated Rpb1 ubiquitination in vitro, we first purified the yeast Paf1$^{(116-445)}$/Leo1 complex (deletion of the

N-terminal Ctr9-binding region in Paf1 does not affect the interaction between Paf1 and Leo1 (47, 51) and is beneficial for the expression and purification of the Paf1$^{(116-445)}$/Leo1 complex) (*SI Appendix*, Fig. S4*A* and lane 1 in *SI Appendix*, Fig. S4*B*). Notably, the purified Paf1$^{(116-445)}$/Leo1 complex promoted Elongin-Cullin complex–mediated Rpb1 ubiquitination in a dose-dependent manner (Fig. 2 *B* and *C*), implying that the Paf1$^{(116-445)}$/Leo1 complex might bind to the Elongin-Cullin complex. Accordingly, we used a co-IP assay and found that Myc-Paf1 and Myc-Leo1 were coimmunoprecipitated by GFP-Elc1-Ela1 but not by GFP-Cul3 (*SI Appendix*, Fig. S4*C*). Additionally, a pulldown assay demonstrated that the Paf1$^{(116-445)}$/Leo1 complex binds to the recombinant Myc-tagged Elc1-Ela1 (Myc-Elc1-Ela1) protein directly (lane 3 in Fig. 2*D*). Moreover,
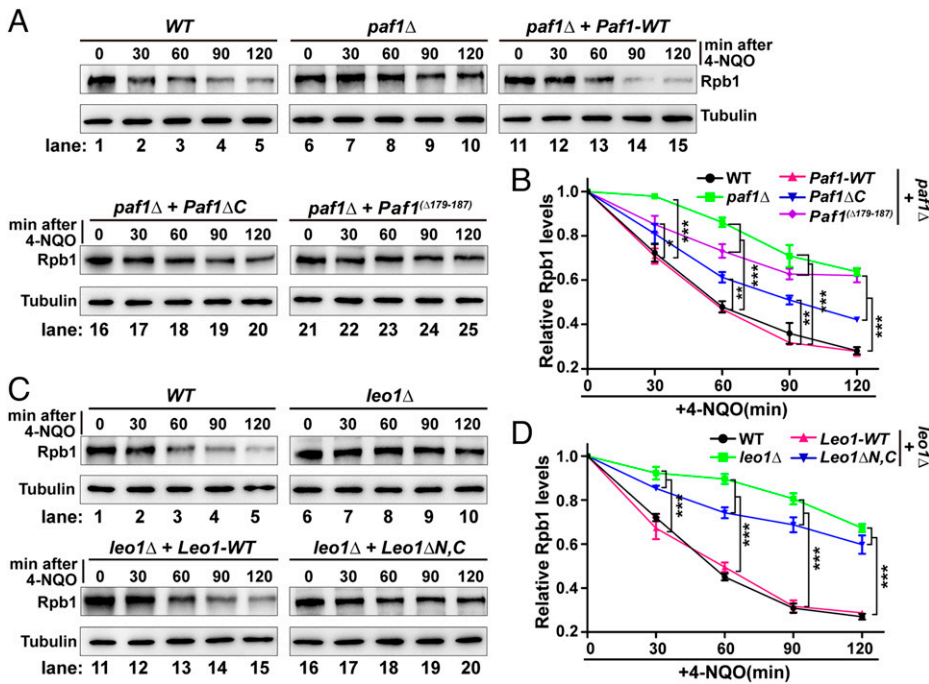
Fig. 4. DNA damage–induced Rpb1 degradation is dependent on the binding of the heterodimer Paf1/Leo1 to Ela1. (*A* and *C*) DNA damage–induced Rpb1 degradation is suppressed in the mutant yeast strains. Logarithmically growing yeast cells were treated with 4-NQO at a final concentration of 5 μg/mL for the indicated times. Samples were prepared by alkaline extraction and analyzed by SDS–PAGE and Western blotting. The 4H8 antibody was used to visualize global Rpb1 protein levels. (*B* and *D*) Quantification of the protein levels of Rpb1 shown in *A* and *C*, respectively. The intensity of the Rpb1 bands was quantified using ImageJ software, and the intensity at time 0 was used for normalization. The error bars indicate the means and SDs (means ± SDs) (*n* = 3 of *A* or *C*, separate experiments). *$P < 0.05$, **$P < 0.01$, ***$P < 0.001$.

we mapped the region on Ela1 involved in binding to the heterodimer Paf1/Leo1. Notably, a co-IP assay clearly demonstrated that full-length Ela1 but not Ela1$^{(1-345)}$ or the other truncations can bind the heterodimer Paf1/Leo1 (*SI Appendix,* Fig. S4D and lanes 3 to 5 in *SI Appendix,* Fig. S4E), indicating that the C-terminal region (aa 345 to 379) of Ela1 is essential for binding to the heterodimer Paf1/Leo1. Consistent with this finding, an in vitro ubiquitination assay showed that the Paf1$^{(116-445)}$/Leo1 complex was able to increase the level of Rpb1 ubiquitination in the presence of the Cul3/Rbx1/Elc1-Ela1 complex (capable of binding to the heterodimer Paf1/Leo1) (lane 3 compared to lane 2 in *SI Appendix,* Fig. S4F; *SI Appendix,* Fig. S4G) but not in the presence of the Cul3/Rbx1/Elc1-Ela1$^{(1-345)}$ complex (incapable of binding to the heterodimer Paf1/Leo1) (lane 5 compared to lane 4 in *SI Appendix,* Fig. S4F; Fig. S4G). Moreover, it is noted that the activity of the Cul3/Rbx1/Elc1-Ela1$^{(1-345)}$ complex is comparable to that of the Cul3/Rbx1/Elc1-Ela1 complex (lane 4 compared to lane 2 in *SI Appendix,* Fig. S4F; *SI Appendix,* Fig. S4G). These results demonstrated that the heterodimer Paf1/Leo1 promotes Elongin-Cullin complex–mediated Rpb1 ubiquitination via an interaction between the heterodimer Paf1/Leo1 and the C-terminal region of Ela1.

Next, we used yeast as a host to test the important role of the binding of Ela1 to the heterodimer Paf1/Leo1 in Elongin-Cullin complex–mediated Rpb1 ubiquitination and degradation in vivo. Notably, following DNA damage, the expression of the Ela1$^{(1-345)}$ mutant (capable of assembling into the Elongin-Cullin complex but incapable of binding to the heterodimer Paf1/Leo1) in the *ela1Δ* strain suppressed Rpb1 ubiquitination (lane 8 compared to lane 7 in Fig. 2*E*) and disrupted Rpb1 degradation (lanes 11 to 15 compared to lanes 1 to 5 in Fig. 2*F*). The protein level of Ela1$^{(1-345)}$ was comparable to that of Ela1-WT (lane 2 compared to lane 1 in *SI Appendix,* Fig. S2A). Together, these results clearly indicated that the interaction between the C-terminal region of Ela1 and the heterodimer Paf1/Leo1 is required for Elongin-Cullin complex–mediated Rpb1 ubiquitination and degradation following DNA damage.

Each Subunit of the Heterodimer Paf1/Leo1 Is Important for Its Binding to Ela1. Prior studies have shown that each subunit of the heterodimer Paf1/Leo1 plays a role in binding histone H3 tails to stimulate Rad6/Bre1-mediated H2Bub (47) or promoting histone turnover to modulate the chromatin state (54). These findings led us to test the role of each subunit of the heterodimer Paf1/Leo1 in binding Ela1. Accordingly, we introduced the Paf1$^{(Δ179-187)}$ mutant (with a β-sheet deletion in Paf1$^{(Δ179-187)}$), which was shown to disrupt the interaction between Paf1 and Leo1 (48), and performed a co-IP assay. Notably, we found that the binding of the Paf1$^{(Δ179-187)}$/Leo1 complex to Ela1 was much weaker than that of the WT Paf1/Leo1 complex (lane 3 compared to lane 2 in Fig. 3*A*; Fig. 3*B*). These results indicated that heterodimer formation is important for the binding of the Paf1/Leo1 complex to Ela1.

Moreover, prior studies showed that the N-terminal region and middle region of Paf1 bind to Ctr9 and Leo1, respectively, and that the middle region of Leo1 binds to Paf1 (Fig. 3*B*; 48, 49, 51). These findings suggested that the C-terminal region of Paf1 and the N-terminal and/or C-terminal region of Leo1 might be involved in binding Ela1. Accordingly, we used a co-IP assay and tested the capacity of two Paf1/Leo1 complexes to bind to Ela1 (Fig. 3*B*). Notably, deletion of either the C-terminal region of Paf1 (Paf1ΔC/Leo1) or both the N-terminal and C-terminal regions of Leo1 (Paf1/Leo1ΔN,C) weakened the interaction between the Paf1/Leo1 complex and Ela1 (Fig. 3*C*, lanes 3 and 4 compared to lane 2; Fig. 3*B*). These results indicated that both Ela1-binding regions in Paf1 and Leo1 are important for the binding of the heterodimer Paf1/Leo1 to Ela1. Additionally, we purified various Paf1/Leo1 complexes—Paf1$^{(116-445)}$/Leo1, Paf1$^{(116-357)}$/Leo1, and Paf1$^{(116-445)}$/Leo1ΔN,C (lanes 1 to 3, respectively, in *SI Appendix,* Fig. S4B)—and tested the capacity of these complexes to promote Elongin-Cullin complex–mediated Rpb1 ubiquitination in vitro. We noted that the Paf1$^{(116-445)}$/Leo1 complex promoted Elongin-Cullin complex–mediated Rpb1 ubiquitination (lane 3 compared to lane 2 in *SI Appendix,* Fig. S4H; *SI Appendix,* Fig. S4I), whereas the Paf1$^{(116-357)}$/Leo1 and the Paf1$^{(116-445)}$/Leo1ΔN,C complexes exhibited a
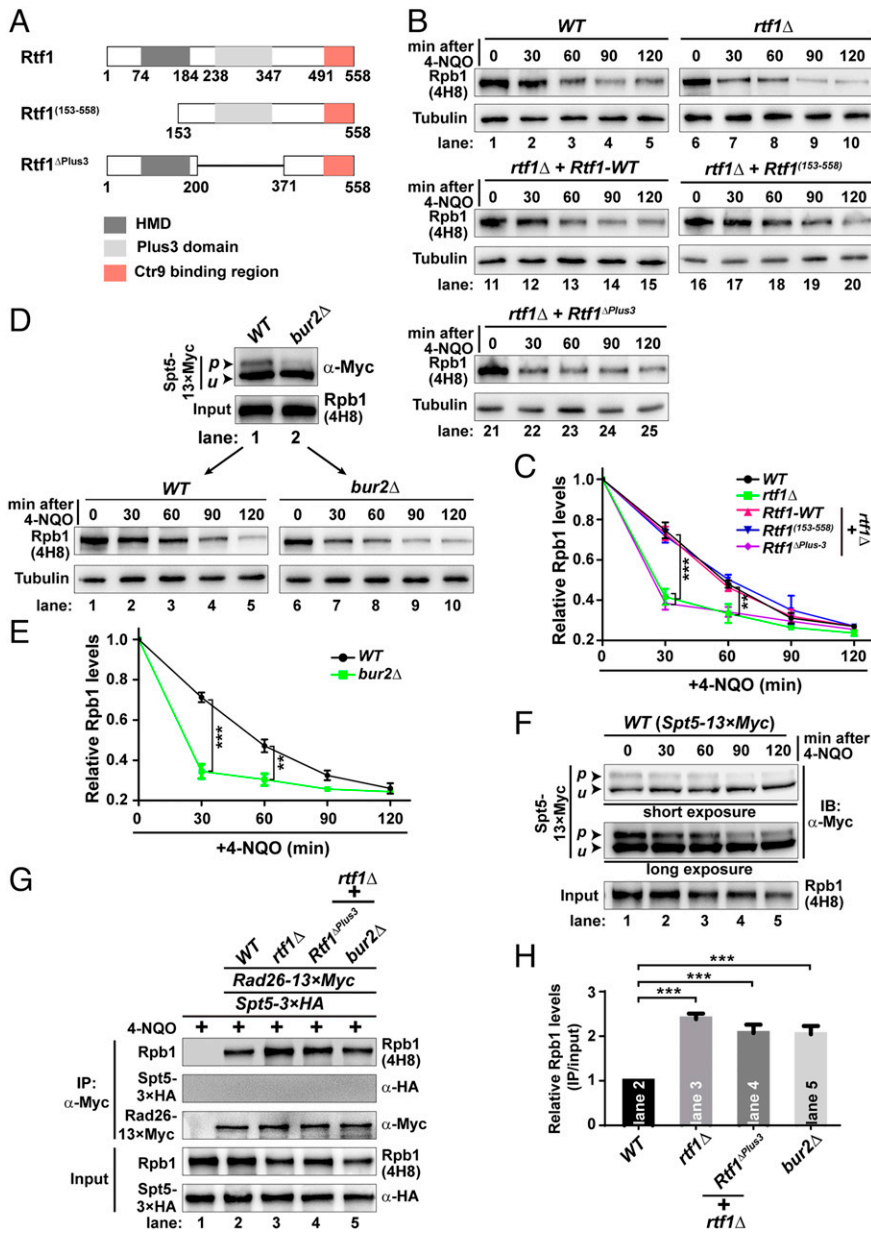
Fig. 5. Decreased binding capacity of Rtf1 to dephosphorylated Spt5 is a critical step in the exchange of Spt5 and Rad26. (*A*) A schematic diagram of full-length Rtf1 and two truncations of Rtf1. The HMD (gray), Plus3 domain (light gray) and Ctr9-binding region (salmon) in Rtf1 are shown. (*B* and *C*) The rate of DNA damage–induced Rpb1 degradation is increased in the *Rtf1^ΔPlus3* strain. Logarithmically growing yeast cells were treated with 4-NQO at a final concentration of 5 μg/mL for the indicated times. Samples were prepared by alkaline extraction and analyzed by SDS–PAGE and Western blotting. The 4H8 antibody was used to visualize global Rpb1 protein levels (*B*). (*C*) Quantification of the protein levels of Rpb1 shown in *B*. The intensity of the Rpb1 bands was quantified using ImageJ software, and the intensity at time 0 was used for normalization. The error bars indicate the means and SDs (means ± SDs) (*n* = 3 of *B*, separate experiments). **P < 0.01, ***P < 0.001. (*D* and *E*) Hypophosphorylation of Spt5 facilitates Rpb1 degradation following DNA damage. The level of phosphorylated Spt5 was decreased in the *bur2Δ* yeast strain (*Upper* panel in *D*). Logarithmically growing yeast cells were treated with 4-NQO at a final concentration of 5 μg/mL for the indicated times. Samples were prepared by alkaline extraction and analyzed by SDS–PAGE and Western blotting. "*p*" and "*u*" indicate phosphorylated and unphosphorylated Spt5, respectively. The 4H8 antibody was used to visualize global Rpb1 protein levels (*Bottom* panel in *D*). (*E*) Quantification of the protein levels of Rpb1 shown in the *Lower* panel of *D*. The intensity of the Rpb1 bands was quantified using ImageJ software, and the intensity at time 0 was used for normalization. The error bars indicate the means and SDs (means ± SDs) (*n* = 3 separate experiments in *D*). **P < 0.01, ***P < 0.001. (*F*) The levels of phosphorylated Spt5 are decreased as Rpb1 degradation progresses following DNA damage. Logarithmically growing yeast strains were treated with 4-NQO at a final concentration of 5 μg/mL for the indicated times. Samples were prepared by alkaline extraction and analyzed by urea-SDS–PAGE in a gel supplemented with 0.01% wt/vol MnCl₂ followed by Western blotting. The anti-Myc antibody was used to visualize Spt5. (*G* and *H*) Disrupting the interaction between Rtf1 and Spt5 facilitates the replacement of Spt5 by Rad26 on stalled RNAPII. (*G*) Co-IP experiments were performed in the indicated yeast strains to evaluate the binding of Rad26-13×Myc to RNAPII or Spt5-3×HA. Logarithmically growing yeast cells were treated with 4-NQO at a final concentration of 5 μg/mL After treatment for 30 min, ~15 optical density at 600 nm units of yeast cells were collected and resuspended in 500 μL of extraction buffer. Whole-cell extracts were prepared by beating with glass beads for 20 min at 4 °C. The *Bottom* panel shows **3%** of RNAPII (indicated by Rpb1) and Spt5-3×HA proteins for each IP. (*H*) Quantitative analysis of the co-IP experimental results is shown in *G*. The intensity of the Rpb1 bands (IP or input) was quantified using ImageJ software, and the band intensity (IP/input) lane 2 was used for normalization. The error bars indicate the means and SDs (means ± SDs) (*n* = 4 separate experiments in *G*). ***P < 0.001.

partial capacity or a complete inability to promote Rpb1 ubiquitination (lane 4 or 5 compared to lane 3 in *SI Appendix*, Fig. S4*H*; *SI Appendix*, Fig. S4*I*).

In addition to Paf1 and Leo1, the conserved multisubunit PAF1C contains three other subunits, as follows: Ctr9, Cdc73, and Rtf1. It is possible that these subunits may also play a role in Elongin-Cullin complex–mediated Rpb1 ubiquitination and degradation by the proteasome following DNA damage. Accordingly, we performed co-IP assays to test the interaction between PAF1C and Elc1-Ela1. As expected, intact PAF1C bound to Elc1-Ela1 (lane 2 in Fig. 3*D*); however, the binding of PAF1C containing mutant Paf1^(Δ179-187) to Elc1-Ela1 was much weaker (lane 4 compared to lane 2 in Fig. 3*D*). Intriguingly, the Elc1-Ela1^(1-345) mutant (incapable of binding to the

heterodimer Paf1/Leo1) did not interact with the intact PAF1C (lane 3 in Fig. 3*D*). Together, these results indicated that the interaction between the C terminus of Ela1 and the heterodimer Paf1/Leo1 is important for the binding of PAF1C to the Elongin-Cullin complex. Moreover, an in vitro ubiquitination assay showed that intact PAF1C promotes Rpb1 ubiquitination much more efficiently than the Paf1^(116-445)/Leo1 complex (lane 4 compared to lane 3 in Fig. 3*E*; Fig. 3*F*). Indeed, available structural and biochemical results indicate that both Ctr9 and Cdc73 have the appropriate surface to interact with yeast RNAPII (55, 56). Collectively, these results indicated that PAF1C might act as a hub for the binding of the Elongin-Cullin E3 ligase complex and the substrate RNAPII by the heterodimer Paf1/Leo1 and either Ctr9 or Cdc73,

respectively, to promote Elongin-Cullin complex–mediated Rpb1 ubiquitination in vitro.

DNA Damage–Induced Rpb1 Degradation Is Dependent on the Binding of the Heterodimer Paf1/Leo1 to Ela1. Both the in vivo and in vitro results clearly showed that the binding of Ela1 to the heterodimer Paf1/Leo1 is crucial for DNA damage–induced Rpb1 ubiquitination and degradation (Fig. 2) and that each subunit of the Paf1/Leo1 heterodimer is important for its binding to Ela1 (Fig. 3). To further investigate the physiological relevance of the Paf1/Leo1 heterodimer's functions following DNA damage, we used yeast as a host to test the effects of mutants of Paf1 and Leo1 in vivo. Notably, we found that DNA damage–induced Rpb1 degradation was completely restored by expression of WT Paf1 (*Paf1-WT*) (lanes 11 to 15 compared to lanes 1 to 5 and 6 to 10 in Fig. 4*A*; Fig. 4*B*) but not by the expression of the Paf1ΔC (with a reduced binding capacity to Ela1) or Paf1$^{(Δ179-187)}$ (incapable of heterodimer formation with Leo1) mutant (lanes 16 to 20 and 21 to 25, respectively, compared to lanes 1 to 5 and 6 to 10 in Fig. 4*A*; Fig. 4*B*) in the *paf1Δ* strain. Consistently, we found that the expression of the Leo1ΔN,C mutant (with a greatly reduced binding capacity to Ela1) in the *leo1Δ* strain did not rescue the rapid Rpb1 degradation induced by DNA damage (lanes 16 to 20 compared to lanes 1 to 5 and 6 to 10 in Fig. 4*C*; Fig. 4*D*). As the control, WT Leo1 (*Leo1-WT*) was expressed in the *leo1Δ* strain (lanes 11 to 15 in Fig. 4*C*; Fig. 4*D*). Moreover, we noted that the protein levels of the Paf1 and Leo1 mutants were comparable to those of WT Paf1 and Leo1, respectively (*SI Appendix*, Fig. S2 *B* and *C*). Together, these in vivo data further confirmed that the specific interaction between the heterodimer Paf1/Leo1 and Ela1 is crucial for Elongin-Cullin–mediated Rpb1 ubiquitination and degradation following DNA damage.

The Ras-Like Domain of Cdc73 Is Important for DNA Damage–Induced Rpb1 Degradation. The in vitro ubiquitination assay showed that intact PAF1C promotes Rpb1 ubiquitination much more efficiently than the Paf1/Leo1 heterodimer (Fig. 3 *E* and *F*), indicating that in addition to Paf1 and Leo1, other subunits in PAF1C might play a role in promoting Rpb1 ubiquitination. Ctr9, as a scaffold protein, is critical for the assembly and functions of PAF1C (47–49, 51) and is also involved in the binding of PAF1C to RNAPII, as indicated by the cryo-electron microscopy (cryo-EM) structures (16, 55). Considering these observations collectively, it is reasonable that the loss of the *CTR9* gene (*ctr9Δ*) in yeast would cause disassembly of PAF1C and thus suppress Rpb1 degradation in response to DNA damage (Fig. 1). Intriguingly, in the *cdc73Δ* yeast strain, Rpb1 degradation was suppressed following DNA damage (Fig. 1), but the mechanism is not clear.

Our recent work showed that Cdc73 is assembled into yeast PAF1C via its middle region (aa 155 to 211, Cdc73$^{(155-211)}$) (51). Cdc73 contains an N-terminal region and a conserved C-terminal Ras-like domain (*SI Appendix*, Fig. S5*A*), both of which are required for the normal level of H2Bub (47). These observations indicated that the N-terminal region and/or the Ras-like domain might contribute to the role of Cdc73 in DNA damage–induced Rpb1 degradation. To this end, we expressed WT Cdc73 (*Cdc73-WT*) and the Cdc73$^{(1-211)}$ and Cdc73$^{(155-393)}$ mutants (both maintaining the capability of assembling into PAF1C, *SI Appendix*, Fig. S5*A*) in the *cdc73Δ* strain and measured the level of Rpb1 degradation in these yeast strains after treatment with 4-NQO. Notably, the expression of either Cdc73-WT or the Cdc73$^{(155-393)}$ mutant

(containing the Ras-like domain) (lanes 11 to 15 or 21 to 25, respectively, compared to lanes 1 to 5 and 6 to 10 in *SI Appendix*, Fig. S5*B*; *SI Appendix*, Fig. S5*C*) but not the Cdc73$^{(1-211)}$ mutant (lacking the Ras-like domain) (lanes 16 to 20 compared to lanes 1 to 5 and 6 to 10 in *SI Appendix*, Fig. S5*B*; *SI Appendix*, Fig. S5*C*) completely rescued the phenotype of Rpb1 degradation, indicating that the C-terminal Ras-like domain of Cdc73 is involved in DNA damage–induced Rpb1 degradation. Consistent with this finding, prior studies showed that the Ras-like domain of Cdc73 binds to the C-terminal domain of Rpb1 (56) and contributes to the recruitment of PAF1C onto chromatin (57). Additionally, we noted a phenotype of reduced efficiency of Rpb1 degradation in the strain expressing Cdc73$^{(1-211)}$ (lanes 16 to 20 compared to lanes 1 to 5 and 6 to 10 in *SI Appendix*, Fig. S5*B*; *SI Appendix*, Fig. S5*C*). It is possible that this phenotype of the *Cdc73$^{(1-211)}$* strain might be related to the partial deficiency of PAF1C binding to RNAPII. Moreover, we noted that the protein levels of Cdc73$^{(155-393)}$ and Cdc73$^{(1-211)}$ were comparable to those of Cdc73-WT (*SI Appendix*, Fig. S2*D*).

PAF1C Interacts with Rad26, a Yeast Ortholog of Human Cockayne Syndrome B (CSB). The above data demonstrated that PAF1C binds to both the Elongin-Cullin E3 ligase complex and the substrate RNAPII, which is indispensable for DNA damage–induced Rpb1 ubiquitination and degradation. Next, we asked the important question of why PAF1C-coordinated Rpb1 degradation occurs specifically in response to DNA damage.

Rad26 is the yeast ortholog of human CSB with ATPase activity. Mutations in CSB are associated with the autosomal recessive neurological disorder Cockayne syndrome, which is characterized by progeroid features, growth failure, and photosensitivity (58, 59). Either Rad26 or CSB is one of the first proteins to be recruited to the sites of DNA lesions in actively transcribed genes to start TCR in an elongating RNAPII-dependent manner (31, 32). Based on these observations combined with cryo-EM structural analyses showing that Rad26 and human PAF1C bind to the upstream DNA and the funnel of RNAPII, respectively (16, 32), in which the C terminus of Leo1 is extended to Rad26 and the Rtf1 Plus3 domain is spatially close to Rad26 (*SI Appendix*, Fig. S6*A*), we speculated that Rad26 might interact with PAF1C via the subunit Leo1 and/or Rtf1 to enhance the recruitment of PAF1C to stalled RNAPII. To test this possibility, we used a co-IP assay. As expected, intact PAF1C was coimmunoprecipitated by GFP-Rad26 (lane 2 or 6 in *SI Appendix*, Fig. S6*B*); the binding affinity of PAF1C for Rad26 was greatly decreased when the Leo1 subunit was absent or replaced by the Leo1ΔN,C mutant (lane 3 or 7 compared to lane 2 or 6, respectively, in *SI Appendix*, Fig. S6*B*). Intriguingly, the absence of Rtf1 did not affect the binding of PAF1C to Rad26 (lane 4 compared to lane 2 in *SI Appendix*, Fig. S6*B*). Consistent with our results, several recent studies also demonstrated that CSB directly interacts with human PAF1C mainly via the Leo1 subunit, not Rtf1, which is important for DNA damage–induced recruitment of more PAF1C to stalled RNAPII (20, 36, 60). Collectively, these data indicated that Rad26 has a role in mediating the DNA damage–induced interaction between PAF1C and stalled RNAPII, which might provide a prerequisite for PAF1C-coordinated specific degradation of Rpb1 induced by DNA damage.

PAF1C and Rad26 Promote Rpb1 Ubiquitination in Concert. We found that the interactions of Ela1 and Rad26 with PAF1C are mainly dependent on the Leo1 subunit and thus

speculated that Rad26 might also bind Ela1 directly. To this end, we performed a pulldown assay and found that Rad26 was pulled down by the recombinant protein Myc-Elc1-Ela1 (lane 3 in Fig. 6A). Moreover, a co-IP assay showed that the Elc1-Ela1$^{(1-143)}$ truncation but not WT Elc1-Ela1 or the Elc1-Ela1$^{(1-345)}$ or Elc1-Ela1$^{(1-277)}$ truncation failed to interact with Rad26 (lane 5 compared to lanes 2 to 4 in Fig. 6B), indicating that the middle region (aa 143 to 277) of Ela1 is important for its binding to Rad26 (see the insert box with the dashed outline in Fig. 6B). Intriguingly, we found that the Rad26-binding region of Ela1 is also required for Ela1 binding to the holo-complex RNAPII (SI Appendix, Fig. S7 A and B) and the summarized results in SI Appendix, Fig. S7D) or the subunit Rpb1 (SI Appendix, Fig. S7C and the summarized results in SI Appendix, Fig. S7D). Consistent with this finding, subsequent co-IP assays further showed that the Ela1$^{(Δ143-277)}$ mutant (deletion of aa 143 to 277) was incapable of binding to Rad26 or RNAPII (SI Appendix, Fig. S7 E and F). Additionally, the in vitro ubiquitination assay showed that the purified Elongin-Cullin E3 ligase complex containing the Ela1$^{(1-143)}$ truncation (lane 4 in SI Appendix, Fig. S8A) but not WT Ela1 or the Ela1$^{(1-345)}$ or Ela1$^{(1-277)}$ truncation (lane 2 or 3, respectively, in SI Appendix, Fig. S8A) failed to ubiquitinate either RNAPII (lane 5 compared to lanes 2 to 4 in SI Appendix, Fig. S8B) or Rpb1 (lane 5 compared to lanes 2 to 4 in SI Appendix, Fig. S8C), indicating that the middle region (aa 143 to 277) of Ela1 is critical for specific substrate recognition by the Elongin-Cullin complex, at least for RNAPII or Rpb1. Together, these results prompted us to consider the possibility that Rad26 and RNAPII competitively interact with Ela1. To exclude this possibility, we used an in vitro ubiquitination assay. Notably, Rad26 efficiently promoted Elongin-Cullin complex–mediated Rpb1 ubiquitination in a dose-dependent manner (Fig. 6 C and D), indicating that Ela1 simultaneously binds to both the important TCR-initiating factor Rad26 and the Elongin-Cullin complex substrate RNAPII via its middle region (aa 143 to 277).

Next, we investigated the role of the middle region of Ela1 in yeast after DNA damage. Notably, the expression of the Ela1$^{(Δ143-277)}$ mutant (capable of assembling into the Elongin-Cullin complex but incapable of binding to Rad26 and recognizing the substrate RNAPII) in the ela1Δ strain diminished Rpb1 ubiquitination (lane 8 compared to lane 7 in Fig. 6E) and disrupted Rpb1 degradation (lanes 11 to 15 compared to lane 1 to 5 in Fig. 6F) after treatment with 4-NQO. Notably, the protein level of Ela1$^{(Δ143-277)}$ was comparable to that of Ela1-WT (lane 3 compared to lane 1 in SI Appendix, Fig. S2A). Moreover, the circular dichroism (CD) spectrums showed that deletion of the middle region of Ela1 (aa 143 to 277) may not result in improper protein folding (SI Appendix, Fig. S8 D and E).

The finding that both PAF1C (Fig. 3 E and F) and Rad26 (Fig. 6 C and D) have the capacity to promote Elongin-Cullin complex–mediated Rpb1 ubiquitination, combined with the observation that PAF1C directly binds to Rad26 (SI Appendix, Fig. S6), suggested that PAF1C and Rad26 might promote Elongin-Cullin complex–mediated Rpb1 ubiquitination in concert. As anticipated, we noted that the level of Rpb1 ubiquitination after the addition of both Rad26 and PAF1C was increased compared to that after the addition of either Rad26 or PAF1C alone (lane 5 compared to lanes 3 and 4 in Fig. 6G; Fig. 6H). Collectively, these results indicated that DNA damage–induced recruitment of the Elongin-Cullin complex to stalled RNAPII at DNA lesions is dependent on PAF1C and Rad26, which are required for Elongin-Cullin complex–mediated Rpb1 ubiquitination and subsequent degradation.

Decreased Binding Capacity of Rtf1 to Dephosphorylated Spt5 Is a Critical Step in the Exchange of Spt5 and Rad26. Prior studies showed that Spt5, as a complex with Spt4, suppresses Rad26-independent TCR in budding yeast (34, 35). Recently, the Patrick Cramer group (36) reported the cryo-EM structure of human RNAPII containing TCR factors and the elongation factors PAF1C and SPT6, revealing that the human DSIF complex (homolog of the yeast Spt4/Spt5 complex) and Rtf1 are replaced by CSB at DNA lesions. Consistent with the behavior of human PAF1C and CSB, our results revealed that the yeast Rtf1 subunit is also not involved in the binding of PAF1C to Rad26 (SI Appendix, Fig. S6B, lane 4 compared to lane 2). However, the mechanism by which the exchange of the DSIF complex and CSB (the Spt4/Spt5 complex and Rad26 in yeast, respectively) is driven in response to DNA damage remains elusive.

Intriguingly, we noted that the rate of DNA damage–induced Rpb1 degradation in the rtf1Δ strain was higher than that in the WT strain (lanes 26 to 30 compared to lanes 1 to 5 in Fig. 1A; Fig. 1B). This phenotype is different from that of strains lacking any one of the other four subunits of PAF1C (Fig. 1), indicating that Rtf1 might play an important role in PAF1C-coordinated RNAPII degradation following DNA damage. Rtf1 contains a Ctr9-binding region and two highly conserved domains, the HMD and Plus3 domains (Fig. 5A). The HMD is critical for PAF1C to promote H2Bub in vivo (47, 61, 62), and the Plus3 domain interacts with the phosphorylated carboxyl-terminal repeat (pCTR) of Spt5 (13, 63, 64), which is required for the recruitment of PAF1C to RNAPII and for fast elongation. Based on these findings, we speculated that the HMD and/or the Plus3 domain of Rtf1 might contribute to the important role of Rtf1 in DNA damage–induced Rpb1 degradation. To test this hypothesis, we used a complementation assay. To evaluate the role of these two domains in DNA damage–induced Rpb1 degradation in vivo, we re-expressed the Rtf1$^{(153-558)}$ (lacking the HMD) or Rtf1^{ΔPlus3} (lacking the Plus3 domain) mutant (Fig. 5A) in the rtf1Δ strain. Our results clearly showed that deletion of the Plus3 domain of Rtf1 (Rtf1$^{(ΔPlus3)}$, lanes 21 to 25 compared to lanes 1 to 5 in Fig. 5B; Fig. 5C) but not deletion of the HMD (Rtf1$^{(153-558)}$, lanes 16 to 20 compared to lane 1 to 5 in Fig. 5B; Fig. 5C) significantly promoted Rpb1 degradation after treatment with 4-NQO. Moreover, we noted that the protein level of each Rtf1 mutant was comparable to that of Rtf1-WT (SI Appendix, Fig. S2E). WT Rtf1 (Rtf1-WT) was expressed in the rtf1Δ strain as the control. These results indicated that the Plus3 domain, not the HMD, of Rtf1 contributes to the role of Rtf1 in DNA damage–induced Rpb1 degradation.

In budding yeast, the Bur1/Bur2 kinase complex is responsible for phosphorylation of the Spt5 CTR, and the pCTR is necessary for Rtf1 binding via the Plus3 domain (13, 63–65). Based on these findings, we speculated that the rate of Rpb1 degradation might be increased in both the rtf1Δ and Rtf1$^{(ΔPlus3)}$ strains after treatment with 4-NQO, most likely because the interaction between the Plus3 domain of Rtf1 and the pCTR of Spt5 is disrupted. To test this hypothesis, we generated a strain with deletion of the BUR2 gene (bur2Δ) and explored the role of Bur2 in DNA damage–induced Rpb1 degradation in vivo. As anticipated, deletion of Bur2 led to a decreased level of Spt5 phosphorylation (lane 2 compared to lane 1 in the Upper panel of Fig. 5D). Intriguingly, we found that the rate of Rpb1 degradation was increased in the strain lacking Bur2 (bur2Δ) compared to that in the WT strain after treatment with 4-NQO (lanes 6 to 10 compared to lanes 1 to 5 in the Lower panel of Fig. 5D; Fig. 5E). These data indicated that dephosphorylation of Spt5 might be triggered by DNA
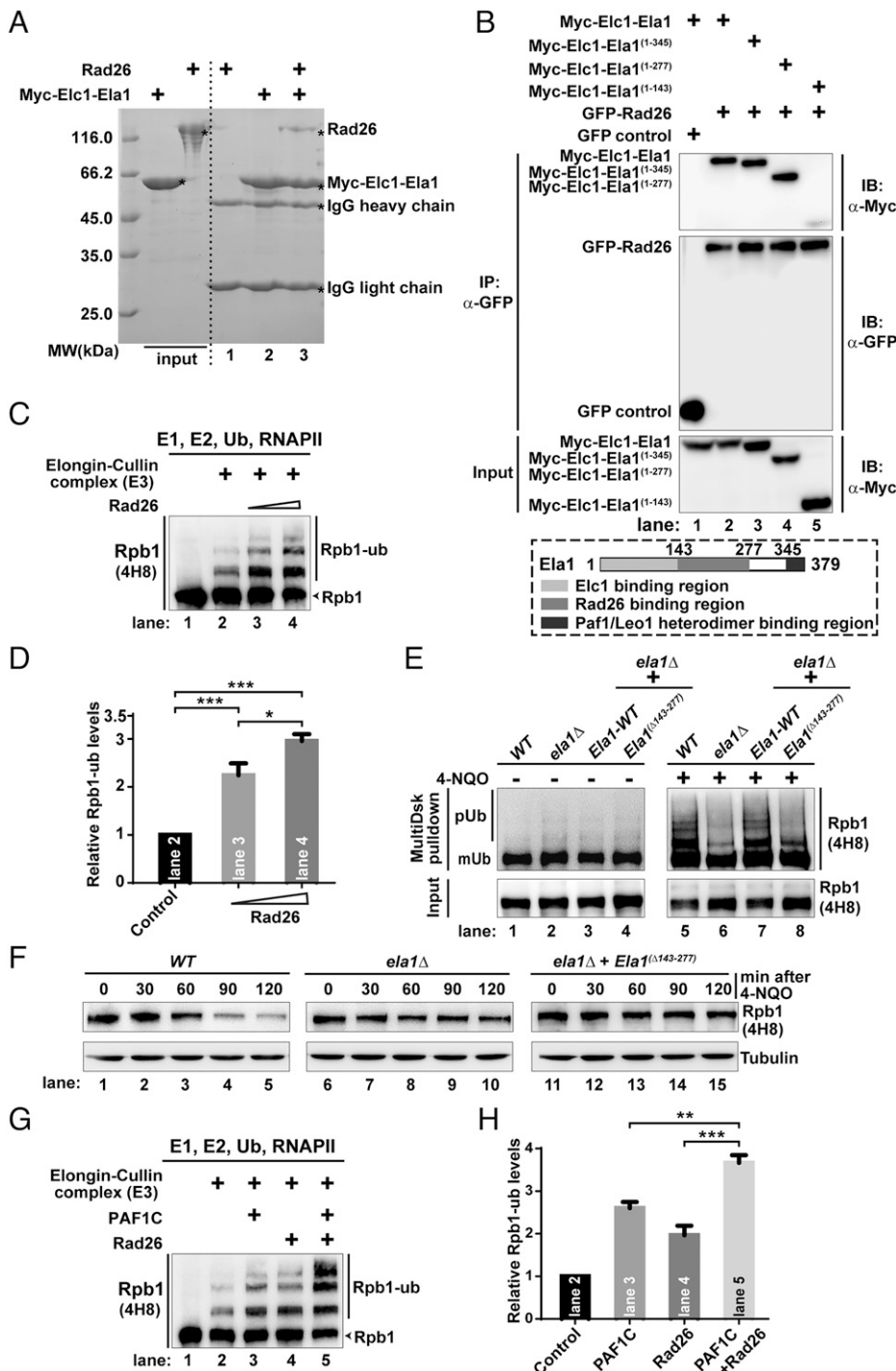
Fig. 6. PAF1C and Rad26 promote Rpb1 ubiquitination in concert. (*A*) Rad26 directly interacts with Elc1-Ela1. Pulldown assays of purified Myc-Elc1-Ela1 with Rad26 were performed. Anti-Myc-tag agarose beads bound to Myc-Elc1-Ela1 were incubated with Rad26 as indicated for 1 h at 4 °C. The prepared samples were separated by SDS–PAGE, and the gel was subjected to Coomassie blue staining. (*B*) The middle region of Ela1 is required for its binding to Rad26. Co-IP experiments were performed to evaluate the binding of Rad26 to full-length or truncated Ela1. Extracts were prepared from HEK293T cells transfected with various combinations of plasmids, as indicated. The *Bottom* panel shows 5% of the Myc-tagged fusion proteins for each IP. A schematic representation of various protein-binding regions of Ela1 is shown in the box enclosed by a dashed line in the *Lower* panel. (*C* and *D*) Rad26 stimulates Elongin-Cullin complex–mediated Rpb1 ubiquitination in a dose-dependent manner. (*C*) An in vitro ubiquitination assay was performed in the presence of incremental amounts of Rad26 (lanes 3 and 4, final concentrations of 1 and 2 μM, respectively). The reactants were incubated for 120 min at 30 °C and analyzed by 6% SDS–PAGE. The membrane was immunoblotted with the 4H8 antibody to specifically detect both Rpb1 and Rpb1-ub. (*D*) Quantitative analysis of the in vitro ubiquitination assay results in *C*. The band intensity of Rpb1-ub was quantified using ImageJ software. A control (lane 2 in *C*) was used for normalization. The error bars indicate the means and SDs (means $\pm$ SDs) ($n = 3$ separate experiments). *$P < 0.05$, ***$P < 0.001$. (*E*) Deletion of the Ela1 middle region suppresses Rpb1 ubiquitination following DNA damage in vivo. GST beads bound to GST-Multi-Dsk2 were incubated with various yeast cell lysates as indicated for 2 h at 4 °C. The prepared samples were separated by SDS–PAGE and then subjected to immunoblotting with the 4H8 antibody to specifically detect Rpb1 ubiquitination. (*F*) Rpb1 degradation is suppressed in the yeast strain lacking the middle region of Ela1 following DNA damage in vivo. Logarithmically growing yeast cells were treated with 4-NQO at a final concentration of 5 μg/mL for the indicated times. Samples were prepared by alkaline extraction and analyzed by SDS–PAGE and Western blotting. The 4H8 antibody was used to visualize global Rpb1 protein levels. (*G* and *H*) PAF1C and Rad26 promote Elongin-Cullin complex–mediated Rpb1 ubiquitination in concert. An in vitro ubiquitination assay was performed in the presence of Rad26 (lane 3), PAF1C (lane 4), or both Rad26 and PAF1C (lane 5). The reactants were incubated for 120 min at 30 °C and analyzed by 6% SDS–PAGE. The membrane was immunoblotted with the 4H8 antibody to specifically detect both Rpb1 and Rpb1-ub. (*H*) Quantitative analysis of the in vitro ubiquitination assay results in *G*. The band intensity of Rpb1-ub was quantified using ImageJ software. A control (lane 2 in *G*) was used for normalization. The error bars indicate the means and SDs (means $\pm$ SDs) ($n = 3$ separate experiments). **$P < 0.01$, ***$P < 0.001$.

damage, which is required for subsequent Rpb1 degradation. Consistent with this finding, we found that the level of phosphorylated but not unphosphorylated Spt5 decreased as Rpb1 degradation progressed in the WT strain expressing 13×Myc-tagged Spt5 (WT (*Spt5-13×Myc*)) after treatment with 4-NQO (Fig. 5*F*). Collectively, these results revealed that disrupting the interaction between Spt5 and Rtf1 by dephosphorylating Spt5 is a critical step in DNA damage–induced Rpb1 degradation.

Prior studies have shown that PAF1C directly interacts with the pCTR of Spt5 mainly via the Rtf1 Plus3 domain in the context of the RNAPII transcriptional machinery for fast elongation (8, 15–17). Combining this finding with our results showing that PAF1C and Rad26 are required for Elongin-Cullin complex loading onto stalled RNAPII at DNA lesions (Figs. 2–4, and 6), along with the interesting observation that Spt5 is replaced by Rad26 in the RNAPII machinery following DNA damage (36), we speculated that either deletion of the Rtf1 subunit (or the Plus3 domain of Rtf1) or loss of Bur2 in the strain might facilitate the replacement of Spt5 by Rad26 on the stalled RNAPII machinery at DNA lesions. To test this hypothesis, we used a co-IP assay to detect the interaction between Rad26-13×Myc and RNAPII or Spt5-3×HA in the
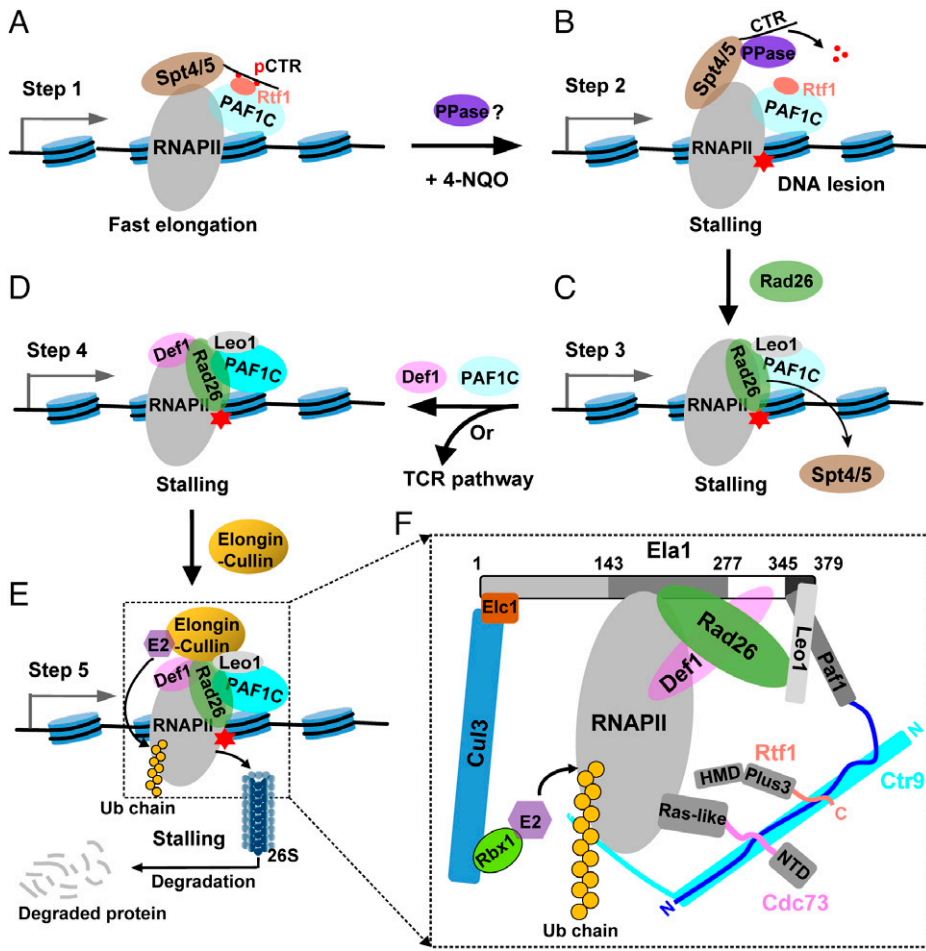
Fig. 7. Schematic model of the mechanism by which yeast PAF1C orchestrates the exchange of Spt5 and Rad26 and the removal of RNAPII. (*A*) In the absence of DNA damage, the Rtf1 subunit (via the Plus3 domain) of PAF1C (colored in pale cyan) interacts with the pCTR of Spt5 in the context of the fast elongation RNAPII machinery. (*B*) In the presence of DNA damage (e.g., induced by 4-NQO treatment), an unknown phosphatase (PPase) is recruited to dephosphorylate the Spt5 pCTR, thus disrupting the interaction between Rtf1 and Spt5 on the damage-stalled RNAPII machinery at DNA lesions, as indicated by the red star. (*C*) Rad26 is loaded to replace the Spt4/Spt5 complex at DNA lesions in an RNAPII-dependent manner, which might be ensured by PAF1C binding. (*D*) Rad26 recruits Def1 and more PAF1C (via binding to the Leo1 subunit) to increase the local concentration of PAF1C (indicated in cyan) at stalled RNAPII. (*E* and *F*) PAF1C, Rad26, and Def1 specifically facilitate the targeting of the Elongin-Cullin complex to stalled RNAPII for its degradation by binding to the C-terminal region (aa 345 to 379), middle region (aa 143 to 277), and (aa 250 to 350) of Ela1, respectively.

WT strain and the *rtf1Δ*, *Rtf1*$^{ΔPlu-3}$ or *bur2Δ* mutant strains after 30 min of 4-NQO treatment (lanes 2 to 5 in Fig. 5*G*). Notably, the amount of Rpb1 coimmunoprecipitated by Rad26-13×Myc in all three mutants was greater than that in the WT strain (lanes 3 to 5 compared to lane 2 in Fig. 5*G*; Fig. 5*H*). However, the signals of Spt5 were not detected in these co-IP assays, indicating that Spt5 was completely absent from RNAPII complexes bound to Rad26 (Fig. 5*G*). A previous study has reported that 15 serines from the first amino acid of 15 copies of a 6-aa repeat at Spt5 CTR are the potential phosphorylation sites (*SI Appendix*, Fig. S9*A* and ref. 13). To further investigate the importance of Spt5 dephosphorylation following DNA damage, we mutated these 15 serines at Spt5 CTR into alanines in yeast (named as *Spt5(15A)*) to prevent phosphorylation of the Spt5 CTR (*SI Appendix*, Fig. S9*A*). Notably, 15A mutations abolished the Spt5 phosphorylation (lane 2 compared to lane 1 in the upper panel of *SI Appendix*, Fig. S9*B*) and modestly facilitated either the DNA damage–induced Rpb1 degradation (lanes 6 to 10 compared to lanes 1 to 5 in the lower panel of *SI Appendix*, Fig. S9*B*; *SI Appendix*, Fig. S9*C*) or the recruitment of Rad26 on the stalled RNAPII (lanes 3 compared to lane 2 in *SI Appendix*, Fig. S9 *D* and *E*).

Collectively, our results uncovered an uncharacterized pathway through which following DNA damage, Spt5 dephosphorylation is induced, thus weakening the interaction between the Rtf1 subunit of PAF1C and Spt5, which modestly facilitates the replacement of Spt5 in the stalled RNAPII machinery by Rad26 at DNA lesions, thereby inducing downstream events such as RNAPII removal (as studied in this report) or TCR.

Discussion

When it encounters a site of DNA damage, the RNAPII machinery undergoes a state transition from fast elongation to stalling for TCR or RNAPII removal, which involves the important event of DSIF replacement by CSB via an undefined mechanism. Intriguingly, PAF1C might participate in the assembly of these two states of the RNAPII machinery, implying that PAF1C might have an important role in orchestrating this complex process. A recent study showed that the CSB-PAF1C axis is required for transcription recovery but not for clearance of DNA lesions by TCR after DNA damage (20). In this report, we showed that PAF1C modulates the exchange of Spt5 and Rad26 and then supports the localization of the Elongin-Cullin E3 ligase complex on stalled RNAPII for degradation in concert with Rad26.

Clearly, the in vitro and in vivo results in this manuscript combined with previous findings uncovered an uncharacterized and multistep pathway for RNAPII removal, as follows. In the absence of DNA damage, binding of the Spt5 pCTR to the Rtf1 subunit (via the Plus3 domain) of PAF1C to recruit PAF1C to the RNAPII machinery is required for fast elongation (8, 13, 15–17) (step 1, Fig. 7*A*). In the presence of DNA damage (e.g., induced by 4-NQO treatment), the RNAPII machinery is stalled at DNA lesions, and an unknown phosphatase (PPase) is recruited to dephosphorylate the Spt5 pCTR, thus disrupting the interaction between Rtf1 and Spt5, which might facilitate the exchange of Spt5 and Rad26 (Fig. 5) (step 2, Fig. 7*B*). Subsequently, Rad26 is loaded to replace the Spt4/Spt5 complex at DNA lesions in a RNAPII-dependent

manner, which might be ensured by PAF1C binding (20, 34–36) (step 3, Fig. 7*C*). And then Rad26 recruits Def1 (41) and more PAF1C (assembled in a Ctr9-mediated manner) to stalled RNAPII by binding to the Leo1 subunit (*SI Appendix,* Fig. S6 and ref. 20) (step 4, Fig. 7*D*). Importantly, PAF1C specifically (via the heterodimer Paf1/Leo1 or the subunit Cdc73) facilitates the targeting of the Elongin-Cullin complex to stalled RNAPII for degradation in concert with Rad26 and Def1 (step 5, Fig. 7 *E* and *F*) (Figs. 2–4 and 6 and ref. 27), or Rad26 promotes TCR pathway activation (31, 32, 35). In this pathway, DNA damage–induced Spt5 dephosphorylation is an interesting observation; it indicates that phosphatase(s) could target Spt5 to dephosphorylate it, which is triggered by DNA damage. It is necessary to identify these phosphatase(s) and the underlying mechanism in the future.

Accumulating studies have shown that Rad26 is a necessary factor in TCR, in which Rad26 first associates with DNA lesions in an RNAPII-dependent manner and subsequently recruits TCR factors to initiate DNA repair (31, 32, 35). However, the role of Rad26 in DNA damage–induced RNAPII removal is ambiguous, as the loss of Rad26 (*rad26Δ*) in strains results in much more efficient Rpb1 degradation (41), consistent with the loss of CSB in human cells (24). One possible explanation for the phenotypes observed in the *rad26Δ* strain is that cells rapidly remove RNAPII to convert active genes into inactive genes and further utilize global genomic repair to remove DNA lesions for cell survival. Our findings showed that PAF1C, in concert with Rad26, specifically localizes the Elongin-Cullin E3 ligase complex to stalled RNAPII for its ubiquitination and subsequent degradation by the proteasome. Consistent with this finding, CSB, the human ortholog of yeast Rad26, regulates the recruitment of the human Elongin-Cullin E3 ligase complex to DNA damage sites (66). Collectively, our results and these previous findings indicate that Rad26 is involved in both the RNAPII removal and TCR pathways. The underlying mechanisms of Rad26 in coordinating these two pathways need to be uncovered in the future.

The results in *SI Appendix,* Fig. S1 indicate that the N-terminal BC-box of Ela1 is critical for Elongin-Cullin complex assembly and DNA damage–induced Rpb1 ubiquitination and degradation. Moreover, our work revealed that Ela1 is a multifunctional scaffold protein that binds simultaneously to RNAPII, Rad26, and PAF1C and that this Ela1-coordinated interaction network is essential for Elongin-Cullin complex–mediated Rpb1 ubiquitination and degradation following DNA damage (Fig. 7 *E* and *F*). Previous results showed that Def1, a Rad26-binding protein, is also required for RNAPII removal by stabilizing the interaction between Ela1 and RNAPII (27). Intriguingly, we found that the Def1-binding region (aa 250 to 350; 27), the PAF1C-binding region (aa 345 to 379), and the Rad26-binding region (aa 143 to 277) of Ela1 are adjacent but not overlapping (Fig. 7*F*), indicating that Def1, PAF1C, and Rad26 might play a cooperative role in RNAPII removal. It seems reasonable that multiple proteins working in concert not only enhance substrate recognition specificity to prevent unnecessary Rpb1 degradation but also improve the reaction efficiency, especially in cells with DNA damage. This hypothesis needs to be tested in future studies.

Materials and Methods

All DNA fragments of proteins involved in this study were amplified from the *Saccharomyces cerevisiae* genome by PCR, and all recombinant complexes were expressed in BL21(DE3)-pUBS520 *Escherichia coli*. For obtaining the *S. cerevisiae* RNAPII, a green fluorescent protein (GFP) was recombined to the C terminus of Rpb3, and RNAPII was purified by one-step purification strategy using agarose beads conjugated with the GFP antibody. An in vitro RNAPII ubiquitination assay was modified and established according to a previous protocol (47). All in vitro ubiquitination assays were repeated at least three times. For visualizing Rpb1 degradation and Spt5 phosphorylation, yeast whole cell extracts were prepared by quick alkaline extraction. For visualizing the ubiquitylated Rpb1, a GST-MultiDsk2 pulldown assay was performed according to a protocol published by the Jesper Q. Svejstrup laboratory (67). The detailed methods for protein expression and purification, analytical ultracentrifugation, protein interaction assays, in vitro RNAPII ubiquitination assay, Rpb1 degradation and ubiquitination or phosphorylated Spt5 detection, Western blotting, and yeast strains can be found in *SI Appendix, SI Materials and Methods*.

Data, Materials, and Software Availability. All study data are included in the article and/or *SI Appendix*.

1. K. Adelman, J. T. Lis, Promoter-proximal pausing of RNA polymerase II: Emerging roles in metazoans. *Nat. Rev. Genet.* **13**, 720–731 (2012).
2. F. X. Chen et al., PAF1, a molecular regulator of promoter-proximal pausing by RNA polymerase II. *Cell* **162**, 1003–1015 (2015).
3. X. Lu et al., Multiple P-TEFbs cooperatively regulate the release of promoter-proximally paused RNA polymerase II. *Nucleic Acids Res.* **44**, 6853–6867 (2016).
4. F. X. Chen et al., PAF1 regulation of promoter-proximal pause release via enhancer activation. *Science* **357**, 1294–1298 (2017).
5. T. Wada et al., DSIF, a novel transcription elongation factor that regulates RNA polymerase II processivity, is composed of human Spt4 and Spt5 homologs. *Genes Dev.* **12**, 343–356 (1998).
6. Y. Yamaguchi et al., NELF, a multisubunit complex containing RD, cooperates with DSIF to repress RNA polymerase II elongation. *Cell* **97**, 41–51 (1999).
7. S. M. Vos, L. Farnung, H. Urlaub, P. Cramer, Structure of paused transcription complex Pol II-DSIF-NELF. *Nature* **560**, 601–606 (2018).
8. L. Wu, L. Li, B. Zhou, Z. Qin, Y. Dou, H2B ubiquitylation promotes RNA Pol II processivity via PAF1 and pTEFb. *Mol. Cell* **54**, 920–931 (2014).
9. M. Yu et al., RNA polymerase II-associated factor 1 regulates the release and phosphorylation of paused RNA polymerase II. *Science* **350**, 1383–1386 (2015).
10. K. Fujinaga et al., Dynamics of human immunodeficiency virus transcription: P-TEFb phosphorylates RD and dissociates negative effectors from the transactivation response element. *Mol. Cell. Biol.* **24**, 787–795 (2004).
11. T. Yamada et al., P-TEFb-mediated phosphorylation of hSpt5 C-terminal repeats is critical for processive transcription elongation. *Mol. Cell* **21**, 227–237 (2006).
12. X. Liu, W. L. Kraus, X. Bai, Ready, pause, go: Regulation of RNA polymerase II pausing and release by cellular signaling pathways. *Trends Biochem. Sci.* **40**, 516–525 (2015).
13. Y. Liu et al., Phosphorylation of the transcription elongation factor Spt5 by yeast Bur1 kinase stimulates recruitment of the PAF complex. *Mol. Cell. Biol.* **29**, 4852–4863 (2009).
14. M. A. Sdano et al., A novel SH2 recognition mechanism recruits Spt6 to the doubly phosphorylated RNA polymerase II linker at sites of transcription. *eLife* **6**, e28723 (2017).
15. L. Hou et al., Paf1C regulates RNA polymerase II progression by modulating elongation rate. *Proc. Natl. Acad. Sci. U.S.A.* **116**, 14583–14592 (2019).
16. S. M. Vos, L. Farnung, A. Linden, H. Urlaub, P. Cramer, Structure of complete Pol II-DSIF-PAF-SPT6 transcription complex reveals RTF1 allosteric activation. *Nat. Struct. Mol. Biol.* **27**, 668–677 (2020).
17. K. Žumer et al., Two distinct mechanisms of RNA polymerase II elongation stimulation in vivo. *Mol. Cell* **81**, 3096–3109.e8 (2021).
18. M. J. Moné et al., Local UV-induced DNA damage in cell nuclei results in local transcription inhibition. *EMBO Rep.* **2**, 1013–1017 (2001).
19. F. Brueckner, U. Hennecke, T. Carell, P. Cramer, CPD damage recognition by transcribing RNA polymerase II. *Science* **315**, 859–862 (2007).
20. D. van den Heuvel et al., A CSB-PAF1C axis restores processive transcription elongation after DNA damage repair. *Nat. Commun.* **12**, 1342 (2021).
21. M. Noe Gonzalez, D. Blears, J. Q. Svejstrup, Causes and consequences of RNA polymerase II stalling during transcript elongation. *Nat. Rev. Mol. Cell Biol.* **22**, 3–21 (2021).
22. M. J. Muñoz et al., DNA damage regulates alternative splicing through inhibition of RNA polymerase II elongation. *Cell* **137**, 708–720 (2009).
23. M. D. Lavigne, D. Konstantopoulos, K. Z. Ntakou-Zamplara, A. Liakos, M. Fousteri, Global unleashing of transcription elongation waves in response to genotoxic stress restricts somatic mutation rate. *Nat. Commun.* **8**, 2076 (2017).
24. A. Tufegdžić Vidaković et al., Regulation of the RNAPII pool is integral to the DNA damage response. *Cell* **180**, 1245–1261.e21 (2020).
25. M. Ljungman, F. Zhang, Blockage of RNA polymerase as a possible trigger for UV light-induced apoptosis. *Oncogene* **13**, 823–831 (1996).
26. J. Q. Svejstrup, The interface between transcription and mechanisms maintaining genome integrity. *Trends Biochem. Sci.* **35**, 333–338 (2010).

27. M. D. Wilson et al., Proteasome-mediated processing of Def1, a critical step in the cellular response to transcription stress. Cell 154, 983–995 (2013).
28. J. Q. Svejstrup, Rescue of arrested RNA polymerase II complexes. J. Cell Sci. 116, 447–451 (2003).
29. H. Gaillard, A. Aguilera, Transcription coupled repair at the interface between transcription elongation and mRNP biogenesis. Biochim. Biophys. Acta 1829, 141–150 (2013).
30. L. H. Gregersen, J. Q. Svejstrup, The cellular response to transcription-blocking DNA damage. Trends Biochem. Sci. 43, 327–341 (2018).
31. S. Malik et al., Rad26p, a transcription-coupled repair factor, is recruited to the site of DNA lesion in an elongating RNA polymerase II-dependent manner in vivo. Nucleic Acids Res. 38, 1461–1477 (2010).
32. J. Xu et al., Structural basis for the initiation of eukaryotic transcription-coupled DNA repair. Nature 551, 653–657 (2017).
33. W. Wang, J. Xu, J. Chong, D. Wang, Structural basis of DNA lesion recognition for eukaryotic transcription-coupled nucleotide excision repair. DNA Repair (Amst.) 71, 43–55 (2018).
34. B. Ding, D. LeJeune, S. Li, The C-terminal repeat domain of Spt5 plays an important role in suppression of Rad26-independent transcription coupled repair. J. Biol. Chem. 285, 5317–5326 (2010).
35. M. Duan, K. Selvam, J. J. Wyrick, P. Mao, Genome-wide role of Rad26 in promoting transcription-coupled nucleotide excision repair in yeast chromatin. Proc. Natl. Acad. Sci. U.S.A. 117, 18608–18616 (2020).
36. G. Kokic, F. R. Wagner, A. Chernev, H. Urlaub, P. Cramer, Structural basis of human transcription-DNA repair coupling. Nature 598, 368–372 (2021).
37. M. D. Wilson, M. Harreman, J. Q. Svejstrup, Ubiquitylation and degradation of elongating RNA polymerase II: The last resort. Biochim. Biophys. Acta 1829, 151–157 (2013).
38. B. Ribar, L. Prakash, S. Prakash, Requirement of ELC1 for RNA polymerase II polyubiquitylation and degradation in response to DNA damage in Saccharomyces cerevisiae. Mol. Cell. Biol. 26, 3999–4005 (2006).
39. B. Ribar, L. Prakash, S. Prakash, ELA1 and CUL3 are required along with ELC1 for RNA polymerase II polyubiquitylation and degradation in DNA-damaged yeast cells. Mol. Cell. Biol. 27, 3211–3216 (2007).
40. M. Harreman et al., Distinct ubiquitin ligases act sequentially for RNA polymerase II polyubiquitylation. Proc. Natl. Acad. Sci. U.S.A. 106, 20705–20710 (2009).
41. E. C. Woudstra et al., A Rad26-Def1 complex coordinates repair and RNA pol II proteolysis in response to DNA damage. Nature 415, 929–933 (2002).
42. J. A. Jaehning, The Paf1 complex: Platform or player in RNA polymerase II transcription? Biochim. Biophys. Acta 1799, 379–388 (2010).
43. B. N. Tomson, K. M. Arndt, The many roles of the conserved eukaryotic Paf1 complex in regulating transcription, histone modifications, and disease states. Biochim. Biophys. Acta 1829, 116–126 (2013).
44. A. M. Francette, S. A. Tripplehorn, K. M. Arndt, The Paf1 Complex: A keystone of nuclear regulation operating at the interface of transcription and chromatin. J. Mol. Biol. 433, 166979 (2021).
45. J. Poli et al., Mec1, INO80, and the PAF1 complex cooperate to limit transcription replication conflicts through RNAPII removal during replication stress. Genes Dev. 30, 337–354 (2016).
46. S. L. Beaudenon, M. R. Huacani, G. Wang, D. P. McDonnell, J. M. Huibregtse, Rsp5 ubiquitin-protein ligase mediates DNA damage-induced degradation of the large subunit of RNA polymerase II in Saccharomyces cerevisiae. Mol. Cell. Biol. 19, 6972–6979 (1999).
47. F. Chen et al., Biochemical insights into Paf1 complex-induced stimulation of Rad6/Bre1-mediated H2B monoubiquitination. Proc. Natl. Acad. Sci. U.S.A. 118, e2025291118 (2021).
48. X. Chu et al., Structural insights into Paf1 complex assembly and histone binding. Nucleic Acids Res. 41, 10619–10629 (2013).
49. Y. Xie et al., Paf1 and Ctr9 subcomplex formation is essential for Paf1 complex assembly and functional regulation. Nat. Commun. 9, 3795 (2018).
50. P. Deng et al., Transcriptional elongation factor Paf1 core complex adopts a spirally wrapped solenoidal topology. Proc. Natl. Acad. Sci. U.S.A. 115, 9998–10003 (2018).
51. F. Chen et al., Crystal structure of the core module of the yeast Paf1 complex. J. Mol. Biol. 434, 167369 (2022).
52. G. Sanchez, J. Barbier, C. Elie, R. Kiernan, S. Rouquier, PAF1 facilitates RNA polymerase II ubiquitination by the Elongin A complex through phosphorylation by CDK12. bioRxiv [Preprint] (2020). https://doi.org/10.1101/2020.09.17.29796. Accessed 17 September 2020.
53. T. Yasukawa et al., Mammalian Elongin A complex mediates DNA-damage-induced ubiquitination and degradation of Rpb1. EMBO J. 27, 3256–3266 (2008).
54. L. Sadeghi, P. Prasad, K. Ekwall, A. Cohen, J. P. Svensson, The Paf1 complex factors Leo1 and Paf1 promote local histone turnover to modulate chromatin states in fission yeast. EMBO Rep. 16, 1673–1687 (2015).
55. Y. Xu et al., Architecture of the RNA polymerase II-Paf1C-TFIIS transcription elongation complex. Nat. Commun. 8, 15741 (2017).
56. H. Qiu, C. Hu, N. A. Gaur, A. G. Hinnebusch, Pol II CTD kinases Bur1 and Kin28 promote Spt5 CTR-independent recruitment of Paf1 complex. EMBO J. 31, 3494–3505 (2012).
57. C. G. Amrich et al., Cdc73 subunit of Paf1 complex contains C-terminal Ras-like domain that promotes association of Paf1 complex with chromatin. J. Biol. Chem. 287, 10863–10875 (2012).
58. K. M. Weidenheim, D. W. Dickson, I. Rapin, Neuropathology of Cockayne syndrome: Evidence for impaired development, premature aging, and neurodegeneration. Mech. Ageing Dev. 130, 619–636 (2009).
59. V. Laugel, Cockayne syndrome: The expanding clinical and mutational spectrum. Mech. Ageing Dev. 134, 161–170 (2013).
60. V. Tiwari, T. Kulikowicz, D. M. Wilson III, V. A. Bohr, LEO1 is a partner for Cockayne syndrome protein B (CSB) in response to transcription-blocking DNA damage. Nucleic Acids Res. 49, 6331–6346 (2021).
61. A. S. Piro, M. K. Mayekar, M. H. Warner, C. P. Davis, K. M. Arndt, Small region of Rtf1 protein can substitute for complete Paf1 complex in facilitating global histone H2B ubiquitylation in yeast. Proc. Natl. Acad. Sci. U.S.A. 109, 10837–10842 (2012).
62. S. B. Van Oss et al., The histone modification domain of Paf1 complex subunit Rtf1 directly stimulates H2B ubiquitylation through an interaction with Rad6. Mol. Cell 64, 815–825 (2016).
63. M. K. Mayekar, R. G. Gardner, K. M. Arndt, The recruitment of the Saccharomyces cerevisiae Paf1 complex to active genes requires a domain of Rtf1 that directly interacts with the Spt4-Spt5 complex. Mol. Cell. Biol. 33, 3259–3273 (2013).
64. A. D. Wier, M. K. Mayekar, A. Héroux, K. M. Arndt, A. P. VanDemark, Structural basis for Spt5-mediated recruitment of the Paf1 complex to chromatin. Proc. Natl. Acad. Sci. U.S.A. 110, 17290–17295 (2013).
65. K. Zhou, W. H. Kuo, J. Fillingham, J. F. Greenblatt, Control of transcriptional elongation and cotranscriptional histone modification by the yeast BUR kinase substrate Spt5. Proc. Natl. Acad. Sci. U.S.A. 106, 6956–6961 (2009).
66. J. C. Weems et al., Cockayne syndrome B protein regulates recruitment of the Elongin A ubiquitin ligase to sites of DNA damage. J. Biol. Chem. 292, 6431–6437 (2017).
67. A. Tufegdzic Vidakovic et al., Analysis of RNA polymerase II ubiquitylation and proteasomal degradation. Methods 159–160, 146–156 (2019).